ORIGINAL ARTICLE

Biosynthesis of silver nanoparticles by *Cyperus pangorei* and its potential in structural, optical and catalytic dye degradation

C. Parvathiraja[1] · S. Shailajha[1] · S. Shanavas[2] · J. Gurung[3]

Abstract

The development of effective photocatalyst through green and eco-friendly approach has become a great concern for the light-induced degradation of organic pollutant dyes. This article reports a simple, cost-effective, and a benign environmental biosynthesis of Ag nanoparticles (NPs) using *Cyperus pangorei*, a plant extract with three different concentrations of $AgNO_3$ in aqueous media. The synthesized silver nanoparticles were performed ultraviolet–visible spectroscopy (UV–Vis), Fourier-transform infrared spectroscopy (FTIR), X-ray diffraction (XRD), photoluminescence (PL), transmission electron microscope (TEM), energy-dispersive X-ray spectroscopy (EDX) and X-ray photoelectron spectroscopy (XPS). The surface plasmon resonance (SPR) peak at 437 nm in UV–Vis spectroscopy confirmed the reduction of Ag^+ ions into Ag nanoparticles. FTIR spectra revealed that plant extract could reduce/stabilize/capping to form Ag nanoparticles, and strong PL emission spectra tend to exhibit higher photocatalytic activity. The structural information is derived from XRD and TEM, which can exhibit the FCC structure and polydisperse with the spherical shape. EDX addresses the presence of Ag constitute. XPS confirmed the Ag nanoparticles in characteristic silver peaks, plant extract derivatives, and their oxidative states' binding energy. The photocatalytic activity of Ag nanoparticles against dye Rhodamine B (Rh-B) under ultraviolet irradiation with periodic interval and pseudo-first-order kinetics were also studied. The obtained results show that the synthesized Ag nanoparticles can degrade dye (Rh-B) up to 86% within 2 h of irradiation time. Furthermore, the present study suggests that the biosynthesized Ag nanoparticles could be potential photocatalysts against various industrial dyes as well as *C. pangorei*; plant extract can be usto modify and develop more efficient nano-photocatalyst for other application.

Keywords Ag NPs · Biosynthesis · *Cyperus pangorei* · Plant extract · Dye Rhodamine B · Photocatalyst · Wastewater treatment · SPR · TEM · XRD

Introduction

In the past few decades, nanomaterials are the forefront of the emerging nanotechnology and nanoscience. It has become the most dynamic interdisciplinary subject among researchers. The nano-sized materials in solid and liquid forms like nanofluids and nanoparticles have versatile applications. The liquid state of nanomaterials is widely used as high heat transfer materials because of their high thermal conductivity and high thermal stability compared to microfluidic materials. Therefore, nanofluids have more vide usability in heat-related fields due to their viscosity, the capacity of storage (nuclear reactor) and density. However, the nanofluids are colloidal dispersion from nanoparticles which is suspended by host fluid, such as oil, water and ethylene glycol. Hence, the researchers are focused on developing the nanoparticles which have better healing properties and also being environmentally friendly (Dadsetani et al. 2020; Bashirnezhad et al. 2016; Ahmadi et al. 2020; Ellahi et al. 2020; Olia et al. 2019; Akbari et al. 2016; Bahmani et al. 2018; Esfahani et al. 2017; Agarwal and Nakara 2019). Often it concerns with control and manipulation of clusters of atoms at nanometric dimensions range in the order of 100 nm (Nouha Bakaraki Turan 2019). Size- and

✉ S. Shailajha
drsshailajha@msuniv.ac.in

1 Department of Physics, Manonmaniam Sundaranar University, Tirunelveli, Tamil Nadu, India

2 Department of Physics, Nano and Hybrid Materials Laboratory, Periyar University, Tamil Nadu, Salem 636 011, India

3 Department of Chemistry, National Institute of Technology Mizoram, Chaltlang, Aizawl 796012, Mizoram, India

shape-dependent function of nanoparticles (NPs) is the key parameter to tune their unique properties (Jamkhandea et al. 2019). Noble metal NPs are more captivating and shown great promising applications in numerous fields like electrocatalyst, photocatalyst, batteries, cancer therapy, etc, (Chhetri et al. 2015; Zheng et al. 2014; Jishma et al. 2018; Yang et al. 2014; Shweta Verma et al. 2019). Such a boost in their application is due to the contribution of large surface area in nano-sized particles which subsequently improves the properties of noble metals (Kelly et al. 2003; Zaniewski et al. 2013; Bastus 2014). Ag NPs with 100 nm dimension usually consist of 20–15,000 silver atoms per particle which possess distinct physical, chemical and biological properties, unlike their bulk materials. Ag NPs have huge potential with substantial interest among the noble metals owing to their unique structural and enhanced physicochemical properties. The better chemical stability as well as high electrical and thermal conductivity with strong oxidation properties (Thakur 2020) make them an ideal element for the favourable electrical interconnector (Sharma et al. 2009). In particular, their unique behaviour manifested in the biological activity which shows them as good candidate for anti-inflammatory, antiviral, antibacterial (Kotp et al. 2019; Kuwabara et al. 2020; Tymoszuk and Miler 2019) antifungal and anticancer activities(Gottesman et al. 2011; Osorio et al. 2012; Monteiro et al. 2012; Krishnaraj et al. 2012; Al-Sheddi et al. 2018). Recently, large-scale production of Ag NPs has also been started, and these synthesized Ag NPs have now become a cheering alternative to traditionally used antibiotic agents due to the release of Ag^+ ions from Ag NPs in the treatment of delayed wounds, burns, ulcers, bladder inflammation and other diseases (Kim 2015; Abdelgawad et al. 2017; Cai et al. 2017; Nazeruddin et al. 2014; Wong and Liu 2010). Moreover, Ag NPs can absorb visible light and regulate the electron density, which is facilitated by surface plasmon resonance (SPR) (Ta et al. 2019). Ag NPs have been found to show their inherent properties for SPR effect and the excitation of localized surface plasmons. They can provide a suitable medium for the detection of surface-enhanced Raman scattering (SERS), which can be used to develop in the analysis of sensitive molecules(Tang et al. (2019)). Besides, simplicity of design and ease of reproducibility for the methods used in Ag NPs synthesis with a wide range of accessible morphologies can be used to obtain unique properties for their application. However, it is hazardous to synthesize the metal NPs through conventional and traditional methods due to the use of harmful and aggressive stabilizing/reducing agents and expensive as well as toxic solvents which are responsible for environmental problems. Since the past decade, a new fashion on the biogenic synthesis (Ravindran et al. 2019) of NPs is underway to meet the green approach or green chemistry and sustainability (Vijaya Kumar et al. 2019; Nazeruddin et al. 2014; Kaushik

Roy et al. 2015a; Jayaseelan et al. 2013; Abolghasem Abbasi Kajani 2014; Roy et al. 2019). Biosynthesis methods using plant extracts are now being viewed as a benign alternative to minimize the outcome from the use of reagents involved in conventional/traditional methods. Furthermore, biosynthesized method (using plant extracts) has immense potential and are more beneficial than other conventional methods and microorganism-based synthesis due to the ease of use, low-cost methods and ease in maintenance of various physical parameters, such as pressure, temperature, etc (Agarwal et al. 2019) Also, in the present scenario, methods for application of single chemical in both stabilizing and reducing agents to control the growth process and effectively tune the size of the NPs are in high demand. Therefore, such a gentle approach has now shifted towards the development of an eco-friendly technique to motivate the biosynthesis of metal NPs for the desired applications.

Mostly, organic dyes are the main ingredient and widely used in dyeing, printing, bleaching and other main processes in the textile industry (Rahimpour et al. 2019). Discharge of effluents containing colours and non-degradable organic chemicals into the environment is of great concern (Akerdi and Hajir Bahrami 2019). Some of the organic dyes like methylene blue, methylene orange, methylene red, congo red, congo rubin, Rh-B, etc., are considered to be environmentally hazardous materials in the same level as other organic pesticides and herbicides (Shanker et al. 2017; Valente et al. 2009; Cao et al. 2008). Among these dyes, Rhodamine B (Rh-B) is commonly used as a family of xanthene's (Khandekara and Bhattacharyya 2019) dyes with fluorescent bluish-red colour and also applied as a biological stain. It has been extensively used in the textile industry due to its low cost, which causes accumulation of Rh-B in industrial wastewater. Their propensity to dissolve in aqueous and protic organic solvents is high and is known for its stability as dye laser materials. Although, at present, the uses of Rh-B from food materials and cosmetic products are illegal due to their toxic and carcinogenic nature. Several methods are frequently used for degradation or removal of hazardous dyes including carbon adsorption, redox treatment, flocculation (Saratale et al. 2011), biological treatment,(Al-Mamun et al. 2019) electro-coagulation, UV photodegradation, micro-reactor, etc, (Nasir et al. 2020; Sarafraz et al. 2019a,b; Goodarzi et al. 2015). However, photocatalysis is the most efficient and cost-effective method. As far as photocatalysts are concerned, noble metal Ag NPs or modified Ag NPs with other metal NPs have already shown promising potential to degrade such hazardous chemicals. It is known that Ag NPs doped with environmentally friendly semiconductor TiO_2 enhance the photocatalytic activity and dye degradation (Cao et al. 2008; Sambaza et al. 2019; Wahyuni et al. 2019; Zhang and Yu 2003; Siddhartha Sankar Boxi and

Santanu Paria 2015). Also, the nanofluids with metals have enhanced catalytic activity. The silver fluids demonstrate the high thermal conductivity, low viscous, which is suited for the cooling system in heat flux set up in the reactor. The previous work reported the parameters of environmental risk assessment considering the outcome and adverse impact of the use of NPs. However, they also mentioned that the environmental impact of Ag is less problematic than metal oxides (Sarafraz et al. 2016,2017,2018a,b, 2019c; Nazari et al. 2020; Sarafraz and Arjomandi 2018; Pourmehran et al. 2018; Wiechers and Musee 2010).

Understanding the importance of efficacy of noble Ag NPs and the effect of hazardous dye like Rh-B to the environment, authors are interested in green chemistry of synthesizing Ag NPs to investigate its photocatalytic activity for the degradation of Rh-B dye. The green approach is adopted using plant extract isolated from *C. pangorei*, and the in situ reduction process of Ag^+ ions into Ag NPs is successfully achieved without adding external capping agents. Treated extracts of *C. pangorei* used for the proposed work possess medicinal worth, and Cyperus family has the largest genera in Cyperaceae with nearly 700 species spread throughout the world (Gupta 2008; Benazir 1993; Jain et al. 2013). *Cyperus pangorei* is a perennial, rhizome decumbent, 3–7 mm thick sedge, clothed with brown scales, with roots of light brown and 0.5–0.7 mm thickness (Simpson et al. 2003; Mayandi et al. 2016a). Results obtained from the characterization of Ag NPs using various techniques, such as UV–Vis spectroscopy, XRD, FT-IR, PL, XPS, TEM and EDX, emphasizes the novelty of using *C. pangorei* aqueous extracted solution for the formation of stable Ag NPs. Further, the photocatalytic activity of the biosynthesized Ag NPs for degradation of dye Rh-B is also studied.
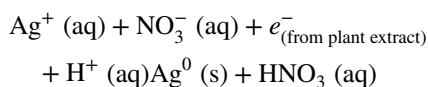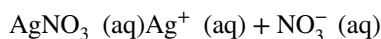
Experimental section

Materials

Silver Nitrate ($AgNO_3$, 99.9% purity) and Rh-B ($C_{28}H_{31}ClN_2O_3$; 99.9% purity) were purchased from HiMedia. The purchased chemicals were used without further purification. All solutions were prepared with double-distilled water, and the specific conductance of double distilled water was found to be 1.5–2 ms cm^{-1} with pH 6.9–7.1. *Cyperus pangorei* plants were collected from Manonmaniam Sundaranar University situated in Tirunelveli District, Tamilnadu, India and was identified with the help of experts in Department of Botany, Manonmaniam Sundaranar University. The collected bundle of the plant was thoroughly washed thrice with tap water and then with double distilled water to remove dust particles.

Preparation of aqueous plant extract

About 15 g (fresh leaves) of plant *C. pangorei* was taken in a round bottom flask with 100 mL of double-distilled water and completely mixed. It was heated at 60 °C for 30 min, and after completion, the solution was kept at room temperature for some time. The extract was filtered through Whatman No.1 filter paper having 11 μm pore size. The supernatant was collected and stored at 4 ºC for further process to synthesis our desired Ag NPs.

Synthesis of Ag nanoparticles

Silver nanoparticles were synthesized in three different sets of $AgNO_3$ solutions in 0.5, 1 and 1.5 mol concentration using 10 mL of plant extract; dissolved in 100 mL double distilled water at room temperature. The solution was stirred at constant rpm in a magnetic stirrer. The colour changes from light green to the dark brownish colour of the solution provide primarily clue for the formation of Ag NPs. The solution was washed in double-distilled water thrice and repeated by centrifuged at 5000 rpm for 10 min. Finally, the precipitate was filtered by Whatman No. 1 filter paper and kept in an oven at 100 °C for 1 h. The samples produced were labelled with A (0.5 mol concentration), B (1 mol concentration) and C (1.5 mol concentration) corresponding to their different molar ratios, respectively. The collected samples were used for further characterization. The reaction and synthesis process depicted as follows in Scheme 1.

$$AgNO_3 \ (aq)Ag^+ \ (aq) + NO_3^- \ (aq)$$

$$Ag^+ \ (aq) + NO_3^- \ (aq) + e^-_{(from \ plant \ extract)} \\ + H^+ \ (aq)Ag^0 \ (s) + HNO_3 \ (aq)$$

Characterization

To detect the localized SPR peak of biosynthesized Ag NPs, UV–Vis spectrophotometric (using Shimadzu UV-2600) technique was employed to measure absorbance spectra. Spectra of prepared samples (A, B and C) were recorded one after another by continuous scanning from 800 to 200 nm, and baseline correction was done using double distilled water as a reference over the similar wavelength range. Measurements of Fourier-transform infrared (FT-IR) spectra (using Perkin Elmer) of the prepared dry sample were achieved within a range of 400–4000 cm^{-1} to identify the different functional groups present on the surface of biosynthesized Ag NPs as well as to analyze the interaction

Scheme 1 The reaction between plant extract (*Cyperus pangorei*) versus silver nitrate. A representation of the Ag NPs synthesis process

between biomolecules and Ag NPs by comparing the shift/nature of the functional peaks. X-ray diffractometer (X-Pert Pro) was used to phase-analyze powder sample. The sample was operated at 60 kV and 40 mA with Cu−Kα radiation ($l = 0.15405$ nm) over 2θ range of 20°–80° through a step size of 0.02 at a scanning rate of 5°/min. Generated XRD peaks matched to the JCPDS data file. Spectrofluorometer PC1 (ISS, USA) was run over the wide range of 800–200 nm to studies the photoluminescence (PL) spectra of prepared Ag NPs. The chemical state of biosynthesized Ag nanoparticles was analyzed using the X-ray photoelectron spectroscopy (XPS, PHI 5000 Versa Probe III, Physical Electronics, USA). Elemental studies were carried out with attached TEM instrument (TITAN) using thermo-energy-dispersive X-ray spectroscopy technique. Such elemental analysis was performed by dispersing the sample over carbon tape, and the sample was sputtered with gold. To analyze TEM (transmission electron microscope) micrograph, the copper grid was prepared with sonicated (10 min) ethanolic solution of the completely dispersed sample. Then, the grid was permitted to dry at ambient circumstances before the TEM analysis.

## Photocatalytic degradation of dye Rh-B by Ag NPs

The comparative studies of biosynthesized Ag NPs (A, B and C) were examined for their photocatalytic activity through degradation of dye Rh-B as a representative pollutant. It was performed under visible light at room temperature. 100 ml of dye Rh-B (10 ppm) was taken in 250 ml beaker, and exact 10 mg of the photocatalyst was added. The

suspension was stirred vigorously in dark exposure for 1 h to attain the adsorption/desorption equilibrium. After an hour, the sample was instantly placed in an ultraviolet chamber using a Xenon lamp. To measure the rate of dye degradation, around 3 ml of solution was taken out into a small centrifuge tube using micropipet at periodic intervals (30 min) and the solution was centrifuged to remove the photocatalyst. Subsequently, the filtrate was placed for analysis using UV–Vis spectroscopy technique to measure the concentration of dye Rh-B through λ_{max} value.

Results and discussion

UV–Vis analysis

The prime importance of our experimental set-up is to synthesize the Ag NPs in aqueous media without using toxic and expensive organic solvents through the in situ reduction of Ag^+ ions into Ag^0 NPs. The procedure was followed by adding *C. pangorei*, plant extract (10 ml) slowly into the chosen aqueous media containing a different concentration of $AgNO_3$ solution (0.5, 1.0 and 1.5 mol concentration) at room temperature. After 1 h, the colour change was observed from light green into dark brownish at fixed rpm. Such visible colour change confirms the change of oxidation state of Ag^+ ions into Ag^0 NPs, and it is known that the exhibition of colour from the electronic spectrum of nanocrystals is due to the coherent excitation of the surface electron within the conduction band known as SPR. It can be easily identified with UV–Vis spectroscopy which is the most widely used
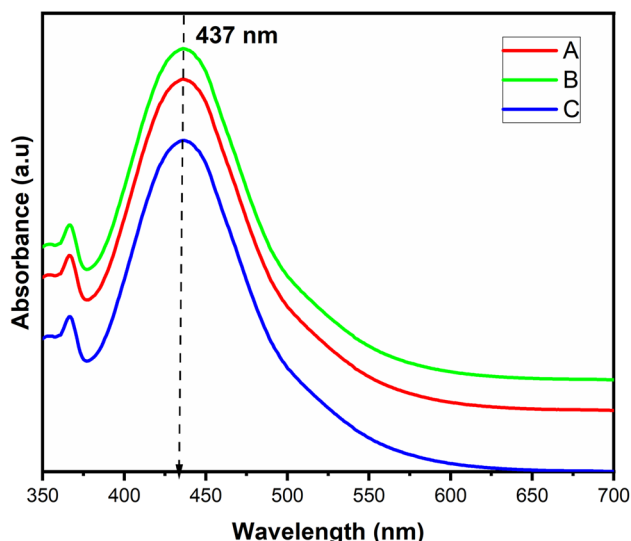
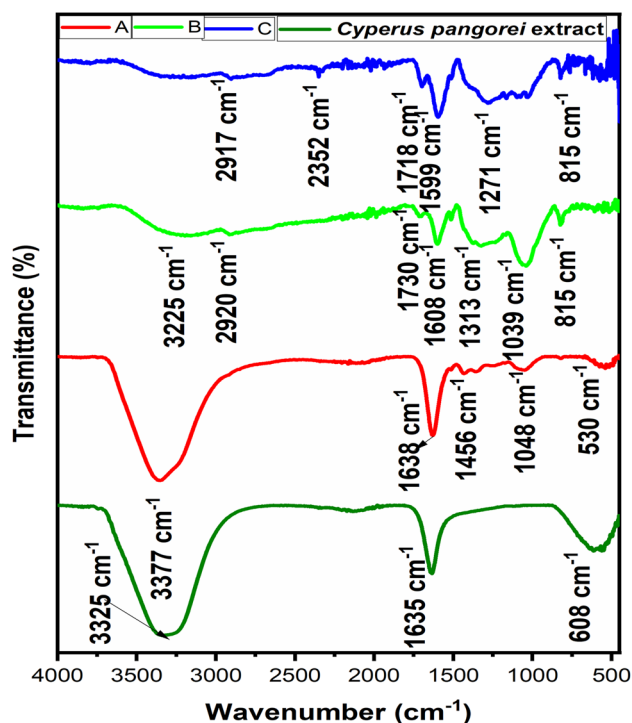**Fig. 1** UV–Vis spectra of biosynthesized Ag NPs (**a–c**)

technique for initial characterization of metal NPs. Typically, Ag NPs exhibit SPR peak in between 400 and 480 nm depending upon the size and shape of the NPs (Flores et al. 2008; Aziz et al. 2015; Rahman et al. 2019).

The obtained electronic spectra from the UV–Vis studies illustrated (Fig. 1) that observed SPR peaks of samples A, B and C are located between 435 and 445 nm confirm the bio-fabrication of Ag NPs. The broadening of the peak between 435 and 480 nm provided notable information for the formation of polydisperse nanoparticles. Normally, two kinds of the broadening of peak or broad band are noticed from Fig. 1. The primary peak from the first band in the ultraviolet region at around 360 nm is responsible for the cluster formation particularly in sample A, and its secondary peak at 440 nm accounted to the formation of Ag NPs. The 360 nm peak represents the higher multipolar excitation due to the presence of SPR with a large size nanoparticles which is authenticated by TEM images (Fig. 5a) (Krishnaprabha and Pattabi 2017). While the other two samples of Ag NPs, i.e., B and C, show similar fashion with slightly different in position of the peak at studied wavelength range. As mole concentration of $AgNO_3$ increases with the fixed amount of plant extract during the synthesis, primary peak or broad band slightly shifted towards lower wavelength (or higher energy) range and secondary peak shifted towards the higher wavelength (or lower energy) range of the spectrum. A synergic effect has been observed for both primary and secondary peaks/bands which compensate for each other. Consequently, it could be correlated with different mole concentration of $AgNO_3$ solution to form Ag NPs by the availability of the fixed amount of capping agent (plant extract) which eventually reflected in size or shape of Ag NPs (Hebeish et al. 2013; Kadam et al. 2019). It is usually

noticed and believed that the SPR peak of NPs shifted to longer wavelength as the size of nanoparticle increases. Capping ability of fixed amount of plant extract (10 mL) may not be sufficient to capped or stabilized Ag NPs in higher mole concentration of $AgNO_3$ solution compared to lower concentration. Consequently, large-sized Ag NPs may be formed which show a shift in secondary SPR peak towards lower wavelength range. Irrespective of quantum yield for the photocatalyst, distribution of absorbed radiation over both wavelength range, i.e., at the ultraviolet and visible region, is a most significant property for the photocatalyst. Furthermore, with a higher absorbance value of sample B at the secondary peak indirectly provides information on the optimization of synthesized Ag NPs for better photocatalytic potential.

FT-IR analysis

Studies of FTIR spectroscopy were carried out to identify the presence of various functional groups of biomolecules at the vicinity of biosynthesize Ag NPs. Measured spectra of samples A, B, C and *C. pangorei* extract are shown in Fig. 2. Previous literature stated that the major component of *C. pangorei* fibres is mainly cellulose (68.5%) from their chemical analysis and remaining are lignin, moisture, ash and wax with 17.8; 9.19, 3.56 and 0.17%, respectively (Sarafraz et al. 2019c). Presence of polyhydroxy group of cellulose is


Fig. 2 FT-IR spectra of biosynthesized Ag NPs (**a–c**) and *Cyperus pangorei* extract

advantageous for the synthesis of metal NPs where it acts as both reducing/stabilizing agents as well as useful to the synthesis of NPs supported by the polymeric matrix (like cellulose) (Benaissi et al. 2010; Ogundare and Zyl 2018; Goswami 2018). The strong intense peaks at 3325, 1635 and 608 cm^{-1} are characteristic of carboxylic acid and C–H deformation of plant molecules. In samples A and B, strong peaks at 3377 and 3225 cm^{-1}, respectively, associated with –O–H stretching vibration of the carboxylic acid group from cellulose component of plant extract (Mayandi et al. 2016b; Shameli et al. 2012). However, a decrease in the intensity of above –O–H stretching vibration moving from sample A to B and for sample C, disappearing or broad band near to that frequency range has been observed. It is indirectly implying that fixed amount of cellulose component of plant extracts with –O–H functional group may be more used in the reduction of Ag$^+$ ions to Ag^0 (from sample A to sample C) and to stabilize the bare Ag NPs. It could be the reason of the disappearing of peak or existence of broad band in sample C (marked by the rectangular box). Following less intense peak at 2917 and 2920 cm^{-1} are corresponded to stretching of C–H and C–H from cellulose (Mayandi et al. 2016b; Shameli et al. 2012). The band at 2352 cm^{-1} region arising from O–H stretching corresponds to the carboxylic acid. Bands at 1718–1730 cm^{-1} carbonyl group of hemicellulose (Mayandi et al. 2016b; Shameli et al. 2012). Similarly, peak responds at 1638, 1608 and 1599 cm^{-1} is due to carbonyl stretching, which indicates the involvement of hemicellulose (Mayandi et al. 2016b). The band at 1456 cm^{-1} is due to phenol groups (Shameli et al. 2012). The bands at 1039 and 1348 cm^{-1} indicate the cyclohexane ring vibration (Kumar 2017). Disappearing of the peak at 1313 cm^{-1} from samples A and B indicated that interaction between the functional group (C–N or –C–N) and Ag ions by the complex formation (Shameli et al. 2012). A band at 1271 cm^{-1} due to the C–N stretching of AgNO$_3$ (Gharibshahi et al. 2017). The weak bands at 815 and 530 cm^{-1} are responsible for the Ag–O vibrations(Gharibshahi et al. 2017). It is known that vibration of the metallic bond between the Ag–Ag bond usually identified below 400 cm^{-1}. As the instrument was run in 400–4000 cm^{-1} range and so, we could not measure the Ag–Ag bond stretching vibration. Therefore, evidence from Fig. 2. could be speculated that plant *C. pangorei* extract is sufficiently enough to reduce Ag$^+$ ions into Ag NPs as well as capped Ag NPs. Further, it brings down into nano-size through the presence of several functional groups, particularly cellulose components.

X-ray diffraction analysis

X-ray diffraction (XRD) studies have been done to examine the crystallographic structure and different phases of the prepared sample. The XRD patterns (Fig. 3) of
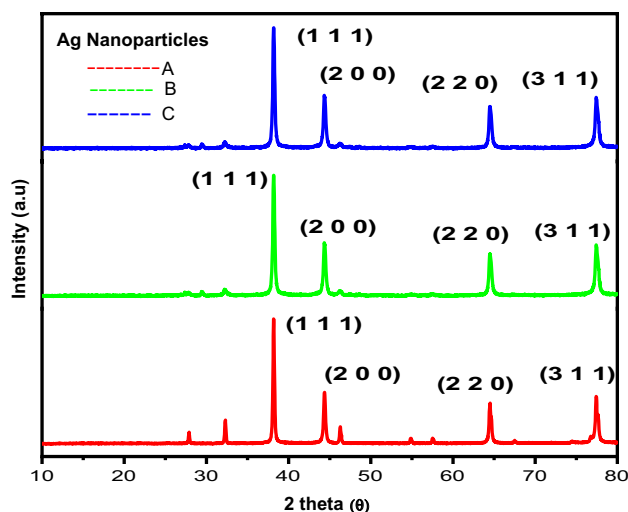
Fig. 3 Powder X-ray diffraction pattern of biosynthesized Ag NPs (**a**–**c**)

biosynthesized Ag NPs (A, B and C) show different intensity with narrow and sharp peaks suggesting that the synthesized samples are good crystalline in nature. It is seen that synthesized Ag NPs are FCC metallic structure of Ag (JCPDS card no: 89-3722) (Kumar et al. 2016) that correspond to the obtained experimental planes as (111), (200), (220) and (311). Our obtained XRD data also matched with previously reported data for the biosynthesized Ag NPs in similar indexed (Wahyuni et al. 2019; Zhang and Yu 2003; Siddhartha Sankar Boxi and Santanu Paria 2015). Particularly, in sample A, some peak with low intensity is noticed below the reflection angle of $2q < 35°$. In contrast, other two samples show in a negligible amount due to remaining of plant extract (as capped molecules) over the surface of Ag NPs or could be interference of impurities like AgO or Ag$_2$O in less/ negligible amount. It is a shred of clear evidence in FT-IR results of the appearance of weak bands at 815 and 530 cm^{-1} due to Ag–O vibrations. However, distinct peaks reflected from the sample are completely clear without much affected by the capping molecules, which imply that the prepared sample belongs to Ag lattice. Intensities in XRD analysis are significant portion to determine the quantitative-phase analysis and to check the unknown crystal structure. The highly intense peaks at Bragg reflection with $2q$ value of 38.194° confirm the promising growth to the face-centered cubic structure of Ag NPs. Furthermore, results obtained with highly intense peak (111) also infer that the interferences of radiation from the plane (111) have more group of atoms which favour the basal plane for the Ag NPs. The crystalline size of the Ag NPs was calculated using the Debye–Scherrer formula to measure the average crystalline size of the sample. It was calculated from the width of XRD peaks employing Scherrer's equation as: $D = \frac{K\lambda}{\beta \mathrm{Cos}\theta}$; where D is average

crystalline domain size, β is the full width at half maximum (FWHM), $K = 0.94$, $\lambda = 0.15405$ nm (wavelength of Cu−Kα radiation) and θ is the diffraction angle. Using broadening of reflection peak (111) from obtained XRD data, average crystalline size of Ag NPs was calculated as 22.67, 22, and 29 nm for samples A, B and C, respectively.

Photoluminescence (PL) analysis

Photoluminescence spectra were recorded for synthesized samples A, B and C, respectively, to examine the optical properties for photocatalytic application. The PL spectra are shown in Fig. 4. It was studied in terms of emission spectra given by the samples and were collected from a wavelength range of 200–800 nm at an excitation (λ_{exc}) wavelength of 340 nm. The nature of optical excitation is another standard condition to get PL spectra for the materials due to proper excitation energy which can select an initial photoexcited state to allow the penetration depth of radiation for the excitation of electrons.

From Fig. 4, distinct peaks were obtained for each sample at around 688 nm (1.806 eV). It has been reported that PL occurred for both the charge/surfactant stabilized gold nanoclusters in relatively intense peak if the size of nanoclusters is sufficiently small (5 nm) (Durston et al. 1997). However, from our XRD finding, it may be concluded that the generation of the less intense peak at around 688 nm either originated from Ag cluster or impurities possessed by Ag NP or vice versa. From UV–Vis spectra, it has been noticed that the formation of some cluster Ag NPs exhibited the broad primary peak. The observed peaks at a different wavelength of PL spectra are responsible for the recombination of excited electrons (as radiative process and a non-radiative
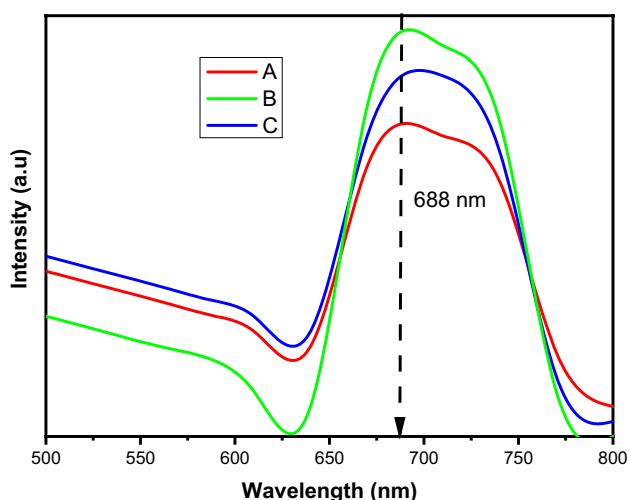
**Fig. 4** Photoluminescence spectra of biosynthesized Ag NPs (A, B and C)

process by a thermal effect) during the process by excitation of wavelength shorter than the most energetic transition of the material. Such electron transition from donor state to acceptor state and containing impurities with sample Ag NPs are also responsible for the transition and consequently associated with appeared peaks. Furthermore, PL spectra strongly depend on surface nanoparticles which are affected by the coupling between surface plasmon and incident light.

From the results, it has been seen that sample B shows highest intense emission peak among the three samples. Such high emission peak could be credited to the promotion of electrons from occupied d bands of Ag NPs due to the absorption of photons into higher electronic states above the Fermi level, consequently leading to electron–phonon and hole–phonon scattering process followed by the energy loss and radiative recombination of an electron from an occupied SP band with the hole (Balaz et al. 2017). Therefore, PL spectra suggest for better performance to influence the photocatalytic property of sample B.

Microscopy analysis using TEM technique

TEM is a powerful tool to characterize sample material on the quantitative scale to measure particles/grain size, particles distribution size as well as morphology. Size and shape are important parameters to determine the intrinsic properties of any NPs. These parameters were studied using the transmission electron microscope technique. For considering the better photocatalytic performance of prepared sample B, here TEM image is provided in Fig. 5a–c to illustrate the size and shape of biosynthesized Ag NPs. From the TEM image, it has been observed that particles are predominately spherical shape with polydisperse. Although a cluster of particles has not been seen from Fig. 5, a portion of the image has some particle at proximity. TEM result shows that Ag NPs seemed to be fine in size and particles' size is distributed from 32 to 60 nm which is believed to be responsible by highly contained cellulose component of *C. pangorei* extract to sufficiently capped Ag NPs. Some previous findings on size and shape of biogenic synthesis of Ag NPs were also matched with obtained shape and size of Ag NPs (Shiv Shankar et al. 2005; Lateef et al. 2015, 2018). From the plot Fig. 6 of frequency count of particles versus particle diameter, maximum counts were observed at 7 nm in the range of 3–14 nm and only small fractions of particle size greater than 20 nm were noticed as shown in the Fig. 5 (inset). The nanoparticles show (Fig. 6a) positively skewed distribution in the range of 2–12 nm which is also agreement with TEM results (Fig. 5b).

Thus, better photocatalytic behaviour may be speculated due to the smaller size (< 20 nm) of the NPs. Analysis of the elemental composition of prepared sample B was carried out using energy-dispersion X-ray (EDX) technique combined
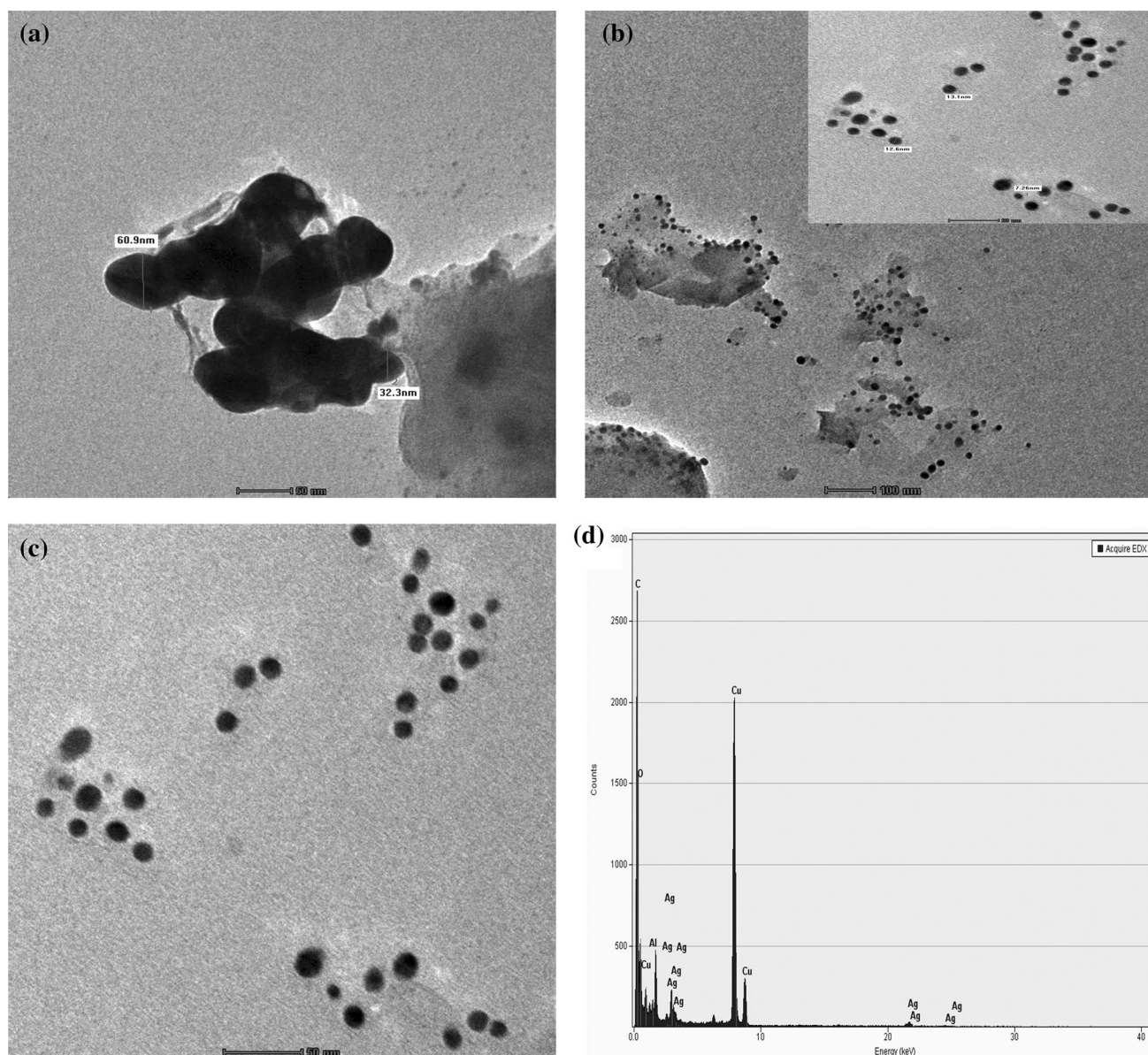
Fig. 5 TEM image of biosynthesized Ag NPs in different magnifications (**a–c**) and EDX spectrum of Ag NPs (**d**)

with TEM instrument. This technique confirms the presence of Ag atoms in prepared Ag NPs, shown in Fig. 5d. From the figure, as expected, Ag element was noticed in prepared composition within the probe region. Usually, Ag NPs show typical optical absorption peak at 3 keV, which is accounted for by the absorption of Ag NPs due to SPR. Therefore, the obtained result from EDX analysis confirms the presence of Ag NPs in the biosynthesized sample. Similarly, the finite presence of oxygen from the peak along with the Ag signal confirms the capping of Ag NPs through oxygen constitutes and some other signals come from the plant extract used, whereas copper and carbon signals were obtained from grid used during the analysis.

X-ray photoelectron spectroscopy analysis

X-ray Photoelectron Spectroscopy examined the synthesized silver nanoparticles (sample B), and their results are shown in Fig. 7. The wide spectrum figure shows the results of C-1s, N-1s, O-1s and Core Ag elements. Figure 7a-d shows the high-resolution XPS spectra of C1s, O1s and Ag 3d core levels. The wide spectrum in N-1s binding energy at 399 eV, which could be attributed to the interaction between the silver nanoparticles and amine groups which is present the *C. pangorei* plant extract. Figure 7b, c indicates the HR-XPS spectrum of C-1s and O-1s. The O-1s peak observed at binding energy 531 eV represents the bond between Ag and O
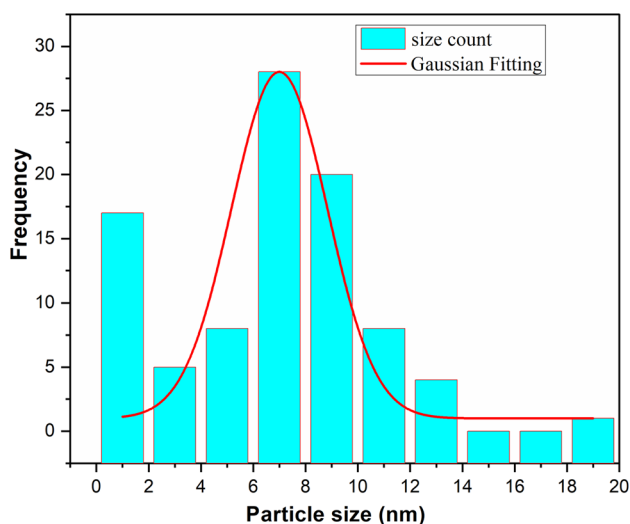
Fig. 6 Histogram of the size distribution of biosynthesized Ag NPs

(Ajitha et al. 2015). The Ag and O bond interactions were formed by the process of a vacancy in d orbital are accumulated by the organic molecules of *C. pangorei* extract.

The binding energies of 283, 285.1 and 287.3 eV indicate the presence of the C–C, C–O and C=O bonds, respectively (Liang et al. 2014). Figure 7d shows the HR-XPS of Ag-3d region in two individual peaks at Ag-3d$_{5/2}$ and Ag-3d$_{3/2}$ can be attributed to 366.6 and 372.6 eV, respectively, which appear due to the spin-orbital splitting in the core level. The doublet splitting of the Ag-3d region binding energy at 6 eV, which indicates the presence of Ag^0 in Ag NPs (Zhang et al. 2008). The XPS results reinsure the FTIR results, which denote the action and reaction of the functional groups and organic components of the *C. pangorei* extract. Both techniques were studied in detail and discussed regarding the synthesis of Ag NPs using *C. pangorei* extract.

Photocatalytic degradation of dye Rh-B

Photocatalytic degradation of hazardous environmental dye, Rh-B was used to explore the photocatalytic efficacy of biosynthesized Ag NPs. It has been analyzed by irradiation of Rh-B solution under ultraviolet light in the presence of sample A, B and C. The time factor is a crucial parameter to remove or degrade pollutants from its source. Therefore, photocatalytic activity was measured using time as a parameter, and kinetic studies have also been done to examine how fast it works. The overall reaction has been monitored to evaluate degradation of dye Rh-B in the presence of sample A, B and C against the irradiation time using UV–Vis spectroscopy technique which is illustrated in Fig. 8. Scheme 2 represents the reaction of the nanoparticles versus dye in the light. The irradiation of light is excited the electrons from the valence band to the conduction band of the Ag NPs due to

the SPR effect. The excited electrons were arrested through the O$_2$ molecules dissolved in the solution and produce superoxides and free radicals. Subsequently, they strongly degrade the harmful particles and dyes. The final product is nontoxic to the environment. Initially, maximum absorbance (λ_{max}) of dye Rh-B is measured without catalyst as well as to correlate with subsequent degradation of dye in the presence of catalyst within an equal periodic interval. In Fig. 8, the aqueous solution of dye without catalyst shows a maximum absorption peak at 557 nm, which is the characteristic peak of Rh-B molecule (Azeez et al. 2018). With passage of time, the intense pink colour of Rh-B in the presence of catalyst slowly becomes faint in colour after the photocatalytic activity of Ag NPs. Furthermore, gradual decreases in absorption maxima of Rh-B have been observed with an increase in the exposure time. Such observed absorbance values are being used, respectively, to evaluate the remaining concentration of Rh-B in the solution.

Results extracted from UV–Vis spectra show that effect of samples A, B and C has a different tendency of photocatalytic activity on the initial concentration of dye Rh-B. Such significant effect on degradation of dye can be seen from the plot of percentage of Rh-B concentration against the irradiation time (Fig. 9). It has been observed that the initial concentration of Rh-B decreases with irradiation time which depends on both the nature of light and photocatalytic potential of synthesized Ag NPs (A, B and C). Throughout the experimental session, no change in Rh-B percentage has been observed in the absence of the catalyst. Mostly degradation of dye takes place due to ultraviolet light-induced process in the presence of Ag NPs. Besides, it is also noticed that the sensitivity of sample B to degrade dye concentration is found to be more throughout the observed time as compared to sample C. In contrast, sample A is found to be the least among the other two. Therefore, the photocatalytic potential of prepared samples to decrease the dye [Rh-B] percentage with passage of time follows the order of sample A < sample C < sample B. Likewise, dye degradation percentage or degradation efficiency of synthesized samples is calculated using the following equation: Degradation (%) = [($C_0 - C_t$)/C_0] × 100; where C_0 is the initial concentration of dye Rh-B solution and C_t is the concentration of the dye solution at t time. The degradation percentages achieved after 120 min of UV light irradiation are found to be 86, 54 and 25% for sample B, sample C and sample A, respectively, with respect to initial concentration of dye Rh-B.
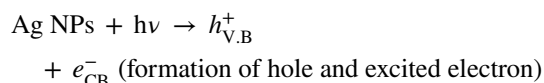
Previously suggested results on the maximum absorbance value at SPR peak and nature of emission peak of sample B through UV–Vis and photoluminescence studies supported our obtained results for the degradation of dye Rh-B. Therefore, sample B showed better photocatalytic potential as compared to the other two samples. Obvious photocatalytic enhancement
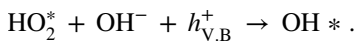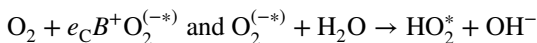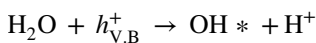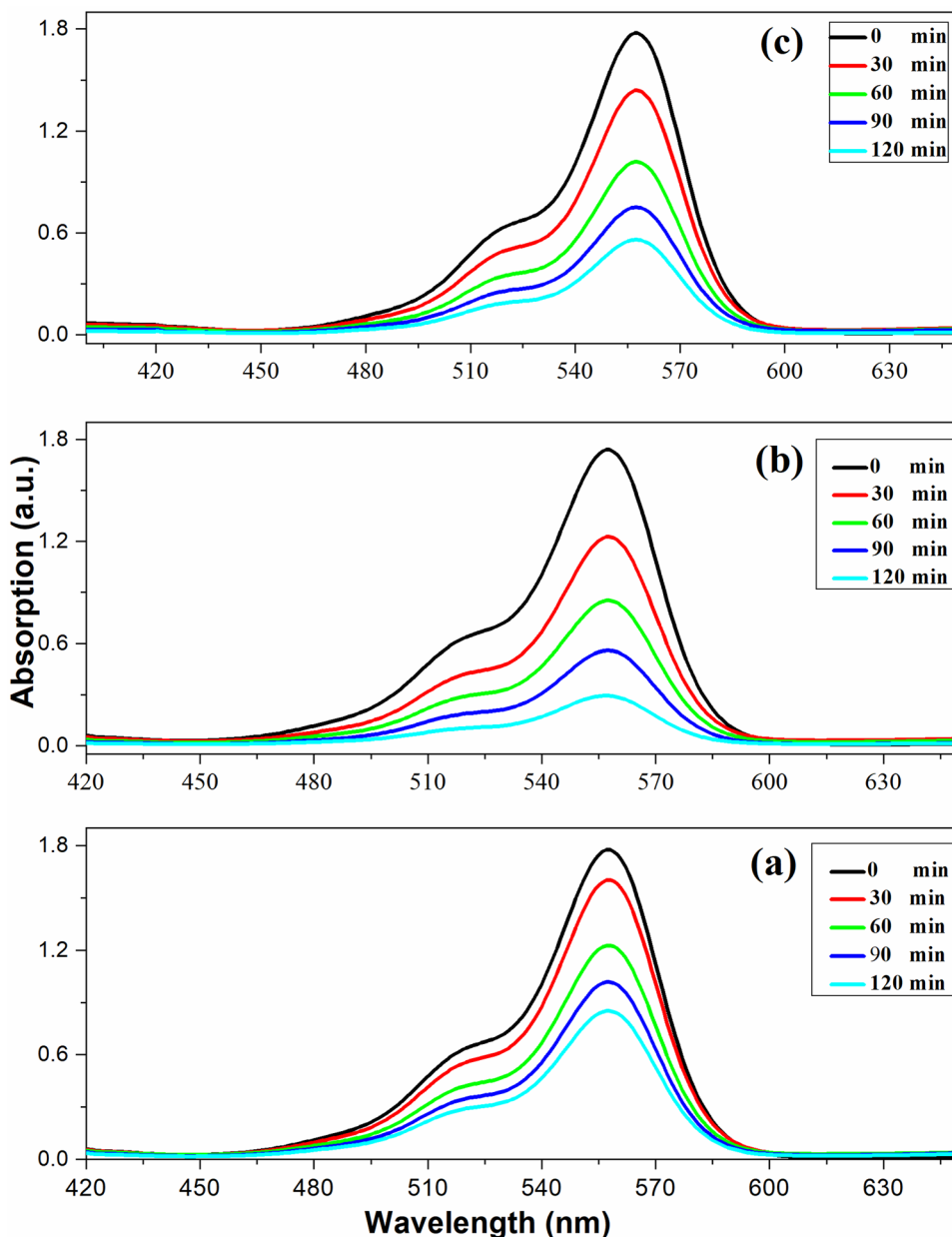
(a)

(b)

(c)

(d)
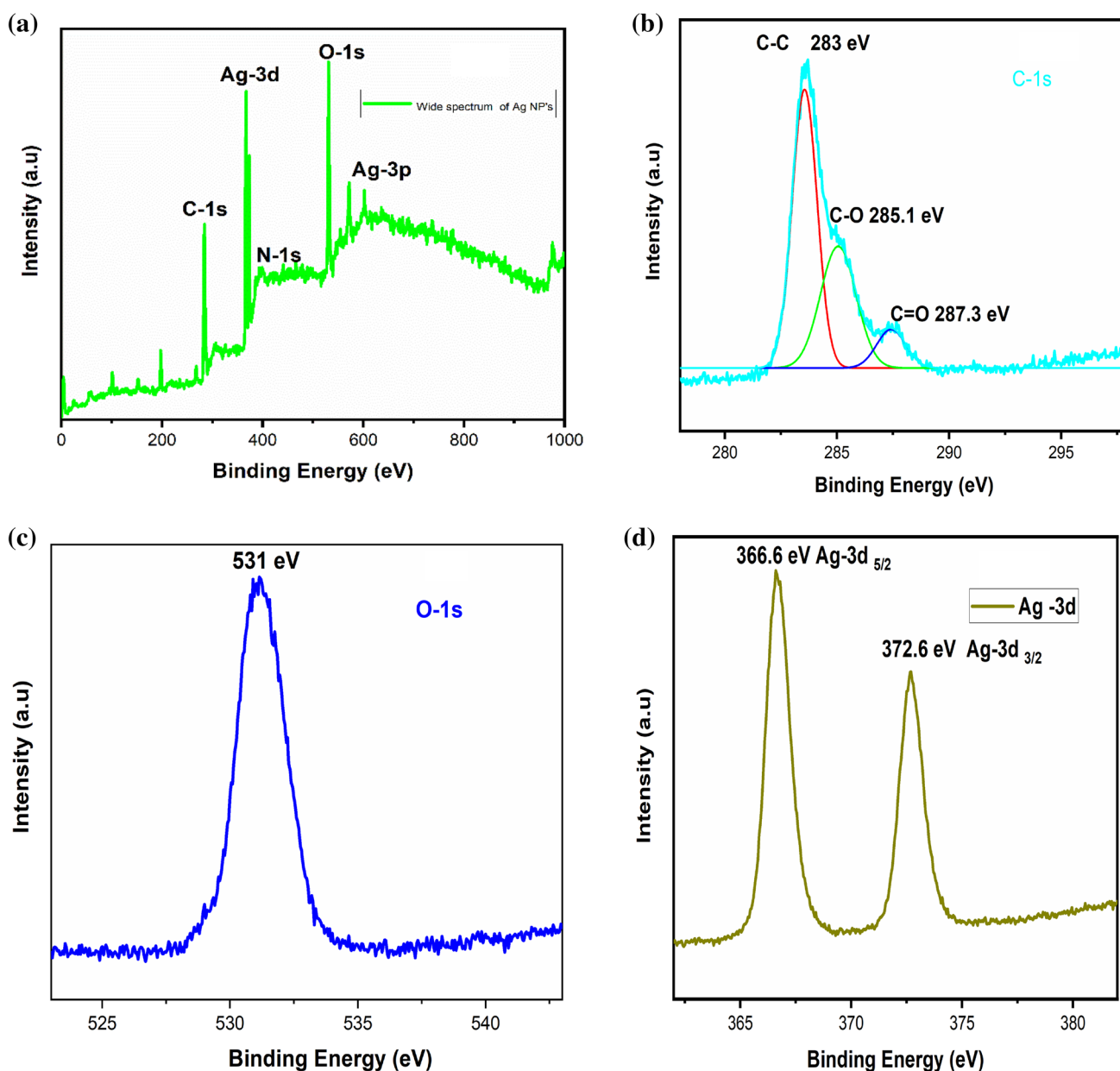
Fig. 7 XPS spectrum for Ag nanoparticles: **a** wide spectrum, **b** C-1s, **c** C-1s, **d** Ag-3d

is responsible for effective excitation of surface plasmon electrons and electron–hole recombination during the UV irradiation process. Furthermore, improved results attributed to the presence of a large surface area of NPs and the interaction of excited surface electrons with the presence of oxygen molecules facilitated the production of hydroxyl radicals in the solution. (Mahmoud et al. 2009; Kaushik Roy et al. 2015b). Interaction of hole with hydroxyl ions can also be responsible for generating reactive species like hydroxyl radicals. These two processes are significant to manifest for the interaction of dye Rh-B molecules and hydroxyl ions to degrade dye molecules. Furthermore, reactive holes can also react with dye
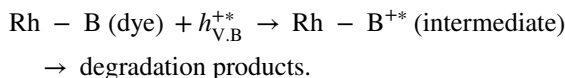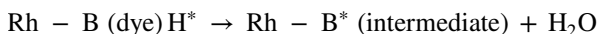
results in the formation of degrade product followed by the oxidation of dye. The mechanism for the absorption of photons by Ag NPs and degradation reaction of the dye Rh-B are supposed to follow as:

$$Ag\ NPs\ +\ h\nu\ \rightarrow\ h^+_{V.B}$$
$$+\ e^-_{CB}\ (formation\ of\ hole\ and\ excited\ electron)$$

$$OH^-\ +\ h^+_{V.B}\ \rightarrow\ OH*\ (formation\ of\ hydroxyl\ radical)$$

Fig. 8 UV–Vis spectra of dye Rhodamine B (Rh-B) in presence of **a** sample A, **b** sample B and **c** sample C at room temperature
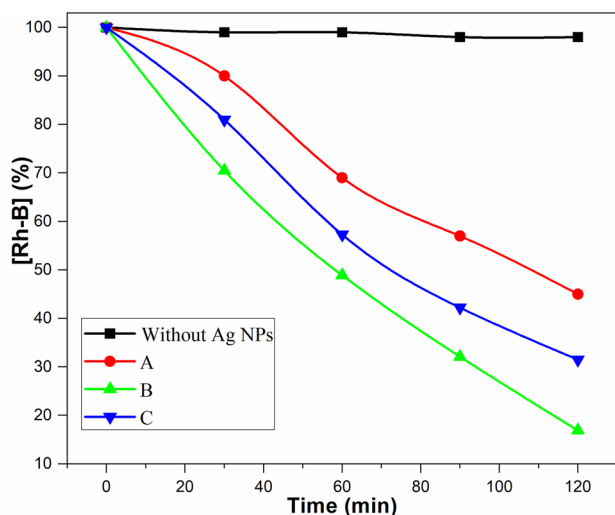

$$H_2O + h_{V.B}^+ \rightarrow OH * + H^+$$

$$O_2 + e_C B^+ O_2^{(-*)} \text{ and } O_2^{(-*)} + H_2O \rightarrow HO_2^* + OH^-$$

$$HO_2^* + OH^- + h_{V.B}^+ \rightarrow OH *.$$

Oxidation of Rh-B via interaction of hydroxyl free radicals is given below:

$$Rh - B \text{ (dye)} H^* \rightarrow Rh - B^* \text{ (intermediate)} + H_2O$$

$$Rh - B \text{ (dye)} + h_{V.B}^{+*} \rightarrow Rh - B^{+*} \text{ (intermediate)}$$
$$\rightarrow \text{ degradation products.}$$

Pseudo-first-order kinetics model was used to study the rate of photocatalytic degradation for dye and it can be expressed by the following equation: $-\ln \left(C_t/C_0 \right) = -kt$, where k is rate constant for the degradation of dye. It can measure from obtained slope by plotting $-\ln \left(C_t/C_0 \right)$ versus dye degradation time (t) and their plots are illustrated in Fig. 10. From pseudo-first-order kinetics model, the rate constants for photocatalytic degradation of Rh-B are found to be 0.098, 0.0115 and
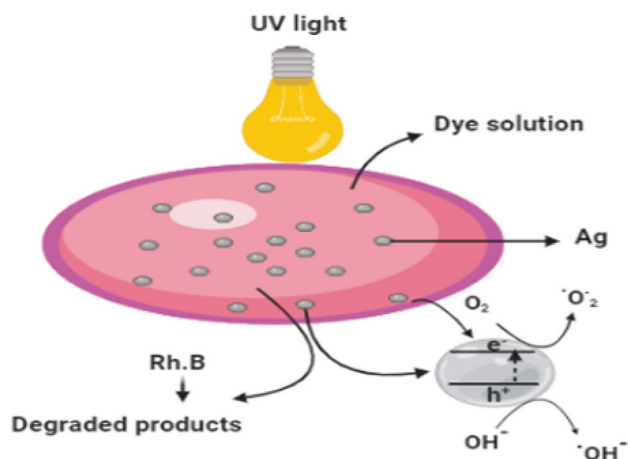
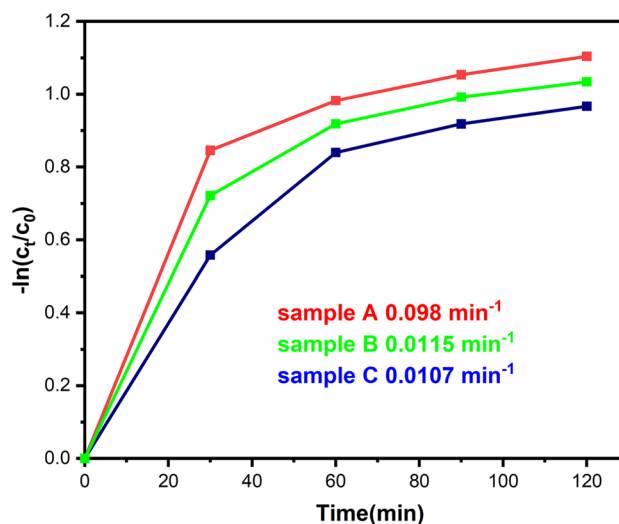Scheme 2 Representation of photocatalytic mechanism of Ag NPs under UV light

Fig. 10 Pseudo first of kinetics degradation of Ag NPs

PL strongly suggests the metal trapping to the photocatalytic activity. From the FTIR spectrum, the cellulose compounds in the plant extract are more responsible in the reduction as well as capping/stabilization of Ag NPs. The photocatalytic activity of the Ag NPs is measured by against the Rh-B dye. The catalytic activity of the Ag NPs sample B could be best in the remaining two samples [B(86%) > C(56%) > A(25%)]. Also, the pseudo-first-order kinetics study revealed that the sample B rate of dye degradation is 1.17346 and 1.0747 times higher than sample A and C, respectively. The plasmonic metals could substantially degrade all kinds of toxic dyes and pollutants. In contrast, the plasmonic metals modified with metal oxides results in the destruction of hazardous pollutants through the photocatalysis method. We concluded the obtained values are advocated that the Ag NPs have more potential for multiple applications.

Compliance with ethical standards

Conflict of interest There are no conflicts to declare.

References

Abdelgawad AM, El-Naggar ME, Eisa WH, Rojas OJ (2017) Clean and high-throughput production of silver nanoparticles mediated by soy protein via solid state synthesis. J Clean Prod 144:501–510

Fig. 9 Plots of (Rh-B) percentage versus irradiation time during the degradation of dye

$0.0107 \ \text{min}^{-1}$ in presence of sample A, sample B and sample C, respectively.

Conclusion

The present study exhibited a simple and cost-effective method on the biosynthesis of Ag NPs using *C. pangorei*, plant extract in aqueous media through the in situ reduction pathway. The UV–Vis spectroscopy confirms the formation of Ag NPs due to the arisen of SPR peak at 435 nm. The synthesized Ag NPs in sample B have higher activity among the other two samples (A, C). The XRD analysis discovered the cubic structure and the TEM studies revealed the spherical morphology of the silver nanoparticles. The wide emission spectrum of

Agarwal H, Nakara A, Shanmugam VK (2019) Anti-inflammatory mechanism of various metal and metal oxide nanoparticles synthesized using plant extracts: a review. Biomed Pharma 109:2561–2572

Agarwal H, Nakara A, Menon S, Shanmugam V (2019) Eco-friendly synthesis of zinc oxide nanoparticles using Cinnamomum Tamala leaf extract and its promising effect towards the antibacterial activity. J Drug Deliv Sci Technol 53:1012

Ahmadi AA, Arabbeiki M, Ali HM, Goodarzi M, Safaei MR (2020) Configuration and optimization of a minichannel using water–alumina nanofluid by non-dominated sorting genetic algorithm and response surface method. Nanomaterials 10(5):901

Ajitha B, Ashok Kumar Reddy Y, Sreedhara Reddy P (2015) Biosynthesis of silver nanoparticles using *Momordica charantia* leaf broth: Evaluation of their innate antimicrobial and catalytic activities. J Photochem Photobiol 146:1–9

Akbari OA, Safaei MR, Goodarzi M, Akbar NS, Zarringhalam M, Shabani GAS, Dahari M (2016) A modified two-phase mixture model of nanofluid flow and heat transfer in a 3-D curved microtube. Adv Powder Technol 27(5):2175–2185

Akerdi AG, Hajir Bahrami S (2019) Application of heterogeneous nano-semiconductors for photocatalyticadvanced oxidation of organic compounds: a review. J Environ Chem Eng 7:103283

Al-Mamun MR, Kaderb S, Islamb MS, Khana MS (2019) Photocatalytic activity improvement and application of UV–TiO2 photocatalysis in textile wastewater treatment: a review. J Environ Chem Eng 7:103248

Al-Sheddi ES, Farshori NN, Al-Oqail MM, Al-Massarani SM, Saquib Q, Wahab R, Musarrat J, Al-Khedhairy AA, Siddiqui MA (2018) Anticancer potential of green synthesized silver nanoparticles using extract of *Nepeta deflersiana* against human cervical cancer cells (HeLA). Bioinorg Chem Appl 15:1–12

Azeez L, Lateef A, Segun A, Abdulrasaq A, Oyedeji O (2018) Novel biosynthesized silver nanoparticles from cob web as adsorbent for Rhodamine B: equilibrium isotherm, kinetic and thermo dynamic studies. Appl Water Sci 8:32

Aziz N, Faraz M, Pandey R, Shakir M, Fatma T, Varma A, Barman I, Prasad R (2015) Facile algae-derived route to biogenic silver nanoparticles: synthesis. Antibact Photocatal Prop Langmuir 31(42):11605–11612

Bahmani MH, Sheikhzadeh G, Zarringhalam M, Akbari OA, Alrashed AA, Shabani GAS, Goodarzi M (2018) Investigation of turbulent heat transfer and nanofluid flow in a double pipe heat exchanger. Adv Powder Technol 29(2):273–282

Balaz M, Balazova L, Putkova NE, Balaxova M, Bujnakova Z (2017) Plant mediated synthesis of silver nanoparticles and their stabilization by wet stirred media milling. Nanoscale Res Lett 12:83

Bashirnezhad K, Bazri S, Safaei MR, Goodarzi M, Dahari M, Mahian O, Wongwises S (2016) Viscosity of nanofluids: a review of recent experimental studies. Int Commun Heat Mass Transfer 73:114–123

Bastus NG, Merkoc P, Piella J, Puntes V (2014) Synthesis of highly monodisperse citrate-stabilized silver nanoparticles of up to 200 nm: kinetic control and catalytic properties. Chem Mater 26:2836–2846

Benaissi K, Johnson L, Walsh DA, Thielemans W (2010) Synthesis of platinum nanoparticles using cellulosic reducing agents. Green Chem 12:220–222

Benazir F (1993) Antimicrobial screening of rhizome extracts of *Cyperus pangorei* Rottb. Pharmacogn Mag 2:80–82

Boxi SS, Paria S (2015) Visible light induced enhanced photocatalytic degradation of organic pollutants in aqueous media using Ag doped hollow TiO2 nanospheres. RSC Adv 5:37657–37668

Cai Y, Piao X, Gao W, Zhang Z (2017) Large-scale and facile synthesis of silver nanoparticles via a microwave method for a conductive pen. RSC Adv 7:34041–34048

Cao Y, Tan H, Shi T, Tang T, Jianqiang (2008) Preparation of Ag-doped TiO2 nanoparticles for photocatalytic degradation of acetamiprid in water. J Chem Tech Biotechnol 83:546–552

Cherie CB, Kagan R, Murray CB (2015) Charge transport in strongly coupled quantum dot solids. Nat Nanotechnol 10:1013–1026

Chhetri M, Rana M, Loukya B, Patil PK, Datta R, Gautam UK (2015) Mechanochemical synthesis of free-standing platinum nanosheets and their electrocatalytic properties. Adv Mater 27:4430–4437

Dadsetani R, Sheikhzadeh GA, Safaei MR, Leon AS, Goodarzi M (2020) Cooling enhancement and stress reduction optimization of disk-shaped electronic components using nanofluids. symmetry 12(6):931

Durston PJ, Schmidt J, Palmer RE, Wilcoxon (1997) Scanning tunneling microscopy of ordered coated cluster layers on graphite. J Appl Phys Lett 71:2940

Ellahi R, Hussain F, Abbas SA, Sarafraz MM, Goodarzi M, Shadloo MS (2020) Study of two-phase newtonian nanofluid flow hybrid with hafnium particles under the effects of slip. Inventions 5(1):6

Esfahani JA, Safaei MR, Goharimanesh M, De Oliveira LR, Goodarzi M, Shamshirband S, Bandarra Filho EP (2017) Comparison of experimental data, modelling and non-linear regression on transport properties of mineral oil based nanofluids. Powder Technol 317:458–470

Flores JC, Torres V, Popa M, Crespo D, Calderón-Moreno JM (2008) Variations in morphologies of silver nanoshells on silica spheres, colloids and surfaces A. Physicochem Eng Aspects 330:86–90

Gharibshahi L, Saion E, Gharibshahi E, Shaari AH, Matori KA (2017) Structural and optical properties of Ag nanoparticles synthesized by thermal treatment method. Materials 10:402

Goodarzi M, Amiri A, Goodarzi MS, Safaei MR, Karimipour A, Languri EM, Dahari M (2015) Investigation of heat transfer and pressure drop of a counter flow corrugated plate heat exchanger using MWCNT based nanofluids. Int Commun Heat Mass Transfer 66:172–179

Goswami M, Moni Das A (2018) Synthesis of cellulose impregnated copper nanoparticles as an efficient heterogeneous catalyst for C–N coupling reactions under mild conditions. Carbohydr Polym 195:189–198

Gottesman R, Shukla S, Perkas N, Solovyov LA, Nitzan Y, Gedanken A (2011) Sonochemical coating of paper by microbiocidal silver nanoparticles. Langmuir 27:720–726

Gupta DP (2008) The herbs habitat morphology and pharmacognosy of medicinal plants, 1st edn. Printwell Offset Publisher, Madhya Pradesh, vol 15, pp 180–181

Hebeish MH, El-Rafie MA, El-Sheikh, El-Naggar ME (2013) Nanostructural features of silver nanoparticles powder synthesized through concurrent formation of the nanosized particles of both starch and silver. J Nanotechnol 2013:10

Jain S, Malviya N, Patidar A (2013) Evaluation of anti-diabetic potential of *Cyperus pangorei* Rottb. ethylacetate subfractions. Int J Pharm Sci 4(7):2746–2752

Jamkhandea PG, Ghule NW, Bamer AH, Kalaskar MG (2019) Metal nanoparticles synthesis: an overview on methods of preparation,advantages and disadvantages, and applications. J Drug Deliv Sci Technol 53:101174

Jayaseelan C, Ramkumar R, Abdul Rahuman A, Perumal P (2013) Green synthesis of gold nanoparticles using seed aqueous extract of *Abelmoschus esculentus* and its antifungal activity. Ind Crops Prod 45:423

Jishma P, NarayananSnigdhaThomasRadhakrishnan RSREK (2018) Rapid degradative effect of microbially synthesized silver nanoparticles on textile dye in presence of sunlight. Biocatal Agric Biotechnol 14:410–417

Kadam D, Momin B, Palamthodi S, Lele SS (2019) Physicochemical and functional properties of chitosan-based nanocomposite films

incorporated with biogenic silver nanoparticles. Carbohydr Polym 211:124–132

Kajani AA, Bordbar A-K, Esfahani SHZ, Khosropour AR, Razmjou A (2014) Green synthesis of anisotropic silver nanoparticles with potent anticancer activity using *Taxus baccata* extract. RSC Adv 4:61394–61403

Kelly KL, Coronado E, Zhao LL, Schatz GC (2003) The optical properties of metal nanoparticles: the influence of size, shape and dielectric environment. J Phys Chem B 107:668–677

Khandekara DC, Bhattacharyya AR, Bandyopadhyaya R (2019) Role of impregnated nano-photocatalyst (SnxTi(1–x)O₂) inside mesoporous silica (SBA-15) for degradation of organic pollutant (Rhodamine B) under UV light. J Environ Chem Eng 7:103433

Kim D-Y, Sung JS, Kim M, Ghodake G (2015) Rapid production of silver nanoparticles at large-scale using gallic acid and their antibacterial assessment. Mat Lett 155:62–64

Kotp AA, Farghali AA, Amin RM, Bdel Moaty SA, El-Deen AG, Gadelhak YM, El-Ela FA, Younes HA, Syame SM, Mahmoud RK (2019) Green-synthesis of Ag nanoparticles and its composite with PVA nanofiber as a promising Cd²⁺ adsorbent and antimicrobial agent. J Environ Chem Eng 7:102977

Krishnaprabha M, Pattabi M (2017) Biogenic synthesis of fluorescent silver nanoparticles using *Melastoma malabathricum* flower extract. AIPC 1832(1):050016

Krishnaraj C, Ramachandran R, Mohan K, Kalaichelvan PT (2012) Optimization for rapid synthesis of silver nanoparticles and its effect on phytopathogenic fungi, Spectrochim. Acta A Mol Biomol Spectrosc 93:95–99

Kumar VA, Uchida T, Mizuki T, Nakajima Y, Katsube Y, Tatsuro H, Maekawa T (2016) Synthesis of nanoparticles composed of silver and silver chloride for a plasmonic photocatalyst using an extract from a weed *Solidago altissima* (goldenrod) Adv. Nat Sci Nanosci Nanonechnol 7:015002121

Kumar B, Smita K, Combol L, Saudi AD (2017) Green synthesis of silver nanoparticles using Andean blackberry fruit extract. J Biol Sci 24:45–50

Kuwabara M, Satob Y, Ishihara M, Takayama T, Nakamura S, Fukuda K, Murakami K, Yokoe H, Kiyosawa T (2020) Healing of *Pseudomonas aeruginosa*-infected wounds in diabetic db/db mice by weakly acidic hypochlorous acid cleansing and silver nanoparticle/chitin-nanofiber sheet covering. Wound Med 28:100183

Lateef A, Ojo SA, Azeez MA, Asafa TB, Yakeen TA, Akinboro A, Oladipo IC, Gueguim EB, Beukes LS (2015) Cobweb as novel biomaterial for the green and eco-friendly synthesis of silver nanoparticle. Appl Nanosci 6:863–874

Lateef A, Adelere IA, Gueguim Kana EB, Asafa TB, Beukes LS (2018) Green synthesis of silver nanoparticles using keratinase obtained from a strain of *Bacillus safensis* LAU 13. Int Nano Lett 5:29–35

Liang S, Zhang G, Min J, Ding J, Jiang X (2014) Synthesis and antibacterial testing of silver/poly (ether amide) composite nanofibers with ultralow silver content. J Nanomater 2014:10

Mahmoud MA, Poncheri A, Badr Y, Abd El Wahed MG (2009) Photocatalytic degradation of methyl red dye. S Afr J Sci 105:299–303

Mayandi V, Rajini N, Pitchipoo P, Winowlin Jappes JT, Varada Rajulu A (2016) Extraction and characterization of new natural lignocellulosic fiber *Cyperus pangorei*. Int J Polym Anal Charact 21:175–183

Monteiro DR, Silva S, Negri M, Gorup LF, de Camargo ER, Oliveira R, Barbosaan DB, Henriques M (2012) Silver nanoparticles: influence of stabilizing agent and diameter on antifungal activity against *Candida albicans* and *Candida glabrata* biofilms. Lett Appl Microbiol 54:383–391

Nasir AM, Jaafar J, Aziz F, Yusof N, Norhayati W, Salleh W, Ismail AF, Aziz M (2020) A review on floating nanocomposite photocatalyst: fabrication andapplications for wastewater treatment. J Water Process Eng 36:101300

Nazari S, Ellahi R, Sarafraz MM, Safaei MR, Asgari A, Akbari OA (2020) Numerical study on mixed convection of a non-Newtonian nanofluid with porous media in a two lid-driven square cavity. J Therm Anal Calorim 140(3):1121–1145

Nazeruddin GM, Prasad NR, Waghmare SR, Garadkar KM, Mullad IS (2014) Extracellular biosynthesis of silver nanoparticle using *Azadirachta indica* leaf extract and its anti-microbial activity. J Alloys Compd 583:272–277

Ogundare SA, van Zyl WE (2018) Nanocrystalline cellulose as reducing- and stabilizing agent in the synthesis of silver nanoparticles: application as a surface-enhanced Raman scattering (SERS) substrate. Surf Interface Anal 13:1–10

Olia H, Torabi M, Bahiraei M, Ahmadi MH, Goodarzi M, Safaei MR (2019) Application of nanofluids in thermal performance enhancement of parabolic trough solar collector: state-of-the-art. Appl Sci 9(3):463

Osorio I, Igreja R, Franco R, Cortez J (2012) Incorporation of silver nanoparticles on textile materials by an aqueous procedure. Mater Lett 75:200–203

Pourmehran O, Sarafraz MM, Rahimi-Gorji M, Ganji DD (2018) Rheological behaviour of various metal-based nano-fluids between rotating discs: a new insight. J Taiwan Inst Chem Eng 88:37–48

Rahimpour M, Taghvaei H, Zafarnak S, Rahimpour MR, Raeissi S (2019) Post-discharge DBD plasma treatment for degradation of organic dye in water: a comparison with different plasma operation methods. J Environ Chem Eng 7:103220

Rahman AU, Khan AU, Yuana Q, Wei Y, AhmadA US, Haq Khan ZU, Shams S, Tariq M, Ahmad W (2019) Tuber extract of Arisaema flavum eco-benignly and effectively synthesize silver nanoparticles: photocatalytic and antibacterial response against multidrug resistant engineered *E. coli* QH4. J Photochem Photobiol B 193:31–38

Ravindran J, Arumugasamy V, Baskaran A (2019) Wound healing effect of silver nanoparticles from *Tridax procumbens* leaf extracts on Pangasius hypophthalmus. Wound Med 27:100170

Roy K, Sarkar CK, Ghosh CK (2015a) Photocatalytic activity of biogenic silver nanoparticles synthesized using yeast (*Saccharomyces cerevisiae*) extract. Appl Nanosci. 5:953–959

Roy K, Sarkar CK, Ghosh CK (2015b) Photocatalytic activity of biogenic silver nanoparticles synthesized using potato (*Solanum tuberosum*) infusion. Spectrochim Acta A 146:286–291

Roy A, Bulut O, Some S, Mandal AM, Deniz Yilmaz M (2019) Green synthesis of silver nanoparticles: biomolecule-nanoparticle organizations targeting antimicrobial activity. RSC Adv 9:2673–2702

Sambaza S, Maity A, Pillay K (2019) Enhanced degradation of BPA in water by PANI supported Ag/TiO₂ nanocomposite under UV and visible light. J Environ Chem Eng 7:102880

Sarafraz MM, Arjomandi M (2018) Demonstration of plausible application of gallium nano-suspension in microchannel solar thermal receiver: experimental assessment of thermo-hydraulic performance of microchannel. Int Commun Heat Mass Transfer 94:39–46

Sarafraz MM, Arya A, Nikkhah V, Hormozi F (2016) Thermal performance and viscosity of biologically produced silver/coconut oil nanofluids. Chem Biochem Eng Q 30(4):489–500

Sarafraz MM, Jafarian M, Arjomandi M, Nathan GJ (2017) Potential use of liquid metal oxides for chemical looping gasification: a thermodynamic assessment. Appl Energy 195:702–712

Sarafraz MM, Arya H, Saeedi M, Ahmadi D (2018) Flow boiling heat transfer to MgO-therminol 66 heat transfer fluid: experimental assessment and correlation development. Appl Therm Eng 138:552–562

Sarafraz MM, Arya H, Arjomandi M (2018) Thermal and hydraulic analysis of a rectangular microchannel with gallium-copper oxide nano-suspension. J Mol Liq 263:382–389

Sarafraz MM, Safaei MR, Goodarzi M, Arjomandi M (2019a) Reforming of methanol with steam in a micro-reactor with Cu–SiO$_2$ porous catalyst. Int J Hydrogen Energy 44(36):19628–19639

Sarafraz MM, Safaei MR, Goodarzi M, Arjomandi M (2019b) Experimental investigation and performance optimisation of a catalytic reforming micro-reactor using response surface methodology. Energy Convers Manage 199:111983

Sarafraz MM, Pourmehran O, Yang B, Arjomandi M (2019) Assessment of the thermal performance of a thermosyphon heat pipe using zirconia-acetone nanofluids. Renew Energy 136:884–895

Saratale RG, Saratale GD, Chang JS, Govindwar SP (2011) Bacterial decolorization and degradation of azo dyes: a review. J Taiwan Inst Chem E 42:138–157

Shameli K, Jazayeri MBASD, Shabanzadeh P, Sangpour P, Gharayebi Y (2012) Investigation of antibacterial properties silver nanoparticles prepared via green method. Chem Cent J 6:73

Shanker U, Rani M, Jassal V (2017) Degradation of hazardous organic dyes in water by nanomaterials. Environ Chem Lett 15:623–642

Sharma VK, Yngard RA, Lin Y (2009) Silver nanoparticles: green synthesis and their antimicrobial activities. Adv Colloid Interfac 145:83–96

Shiv Shankar S, Rai A, Ahmad A, Sastry M (2005) Controlling the optical properties of lemon grass extract synthesized gold nanotriangles and potential applications infrared- absorbing optical coatings. Chem Mater 17(3):566–572

Simpson DA, Furness CA, Hodkinson TR, Mark Chase AMMW (2003) Phylogenetic relationships in cyperaceae subfamily mapanioideae inferred from pollen and plastid DNA sequence data. Am J Bot 90(7):1071–1086

Ta QTH, Cho E, Sreedhar A, Noh J-S (2019) Mixed-dimensional, three-level hierarchical nanostructures of silver and zinc oxide for fast photocatalytic degradation of multiple dyes. J Catal 371:1–9

Tang J, Chen W, Ju H (2019) Rapid detection of pesticide residues using a silver nanoparticles coated glass bead as nonplanar substrate for SERS sensing. Sens Actuat B 287:576–583

Thakur N, Anu A, Kumar K (2020) Effect of (Ag, Co) co-doping on the structural and antibacterial efficiency of CuO nanoparticles: a rapid microwave assisted method. J Environ Chem Eng 8:104011

Turan NB, Erkan HS, Engin GO, Bilgili MS (2019) Nanoparticles in the aquatic environment: usage, properties, transformation and toxicity—a review. Process Saf Environ 130:238–249

Tymoszuk A, Miler N (2019) Silver and gold nanoparticles impact on in vitro adventitious organogenesis in chrysanthemum, gerbera and cape primrose. Sci Hortic 257:108766

Valente JS, Tzompantzi F, Prince J, Cortez JGH, Gomez R (2009) Adsorption and photocatalytic degradation of phenol and 2,4 dichlorophenoxiacetic acid by Mg–Zn–Al layered double hydroxides. Appl Catal B 90:330–338

Verma S, Tirumala Rao B, Jayabalan J, Raid SK, Phasee DM, Srivastavad AK, Kaula R (2019) Studies on growth of Au cube-ZnO core-shell nanoparticles for photocatalytic degradation of methylene blue and methyl orange dyes inaqueous media and in presence of different scavengers. J Environ Chem Eng 7:103–209

Vijaya Kumar P, Mary S, Kala J, Prakash KS (2019) Green synthesis derived Pt-nanoparticles using *Xanthium strumarium* leaf extract and their biological studies. J Environ Chem Eng 7:103146

Wahyuni ET, Roto R, Novarita D, Suwondo KP, Kuswandi B (2019) Preparation of TiO$_2$/AgNPs by photodeposition method using Ag(I) presentin radiophotography wastewater and their antibacterial activity in visible light illumination. J Environ Chem Eng 7:103178

Wiechers JW, Musee N (2010) Engineered inorganic nanoparticles and cosmetics: facts, issues, knowledge gaps and challenges. J Biomed Nanotechnol 6:408–431

Wong KK, Liu X (2010) Silver nanoparticles—the real "silver bullet" in clinical medicine? Med Chem Comm 1(2):125–131

Yang B, Yang Z, Wang R, Feng Z (2014) Silver nanoparticle deposited layered double hydroxide nanosheets as a novel and high performing anode material for enhanced Ni–Zn secondary batteries. J Mater Chem A 2:785–791

Zaniewski AM, Schriver M, Lee JG, Crommie MF (2013) Electronic and optical properties of metal-nanoparticle filled graphene sandwiches. Appl Phys Lett 102:23108–23116

Zhang L, Yu JC, Yip H, Quan HY, Kwong L, Kwon KW, Xu A-W, Wong P-K (2003) Ambient light reduction strategy to synthesize silver nanoparticles and silver-coated TiO$_2$ with enhanced photocatalytic and bactericidal activities. Langmuir 19:10372–10380

Zhang H, Wang G, Chen D, Lv XJ, Li JH (2008) Tuning photoelectrochemical performances of Ag–TiO$_2$ nanocomposites via reduction/oxidation of Ag. Chem Mater 20:6543–6549

Zheng J-N, Lv J-J, Li S-S, Xue M-W, Wang A-J, Feng J-J (2014) One-pot synthesis of reduced graphene oxide supported hollow Ag@Pt core–shell nanospheres with enhanced electrocatalytic activity for ethylene glycol oxidation. J Mater Chem A 2:3445–3451

Publisher's Note Springer Nature remains neutral with regard to jurisdictional claims in published maps and institutional affiliations.